ACS Sustainable Chemistry & Engineering

pubs.acs.org/journal/ascecg

Research Article

Magnesium-Promoted Rapid Nucleation of Carbon Dioxide Hydrates

Aritra Kar, Palash Vadiraj Acharya, Awan Bhati, Ashish Mhadeshwar, Pradeep Venkataraman, Timothy A. Barckholtz, Hugo Celio, Filippo Mangolini, and Vaibhav Bahadur*

Cite This: https://doi.org/10.1021/acssuschemeng.1c03041

Read Online

ACCESS | Metrics & More | Article Recommendations | Supporting Information

ABSTRACT: Gas hydrates offer solutions in areas like CO_2 sequestration and desalination. However, their formation is severely limited by long induction (wait) times for nucleation, which range from hours to days. Many existing nucleation promotion techniques involve chemical additives, which invite environmental and process-related concerns. Here, we report a simple, passive, and environmentally friendly technique to significantly promote the nucleation of CO_2 hydrates: magnesium (in pure and alloy forms) triggers nucleation almost instantaneously. We report induction times of less than 1 min, which is the fastest induction time reported for any gas hydrate under stagnant conditions. This translates to Mg-promoted nucleation rates being 3000 times higher than the baseline. Statistically meaningful measurements of nucleation kinetics (in milliliter and liter-scale reactors), direct visualization of nucleation, and X-ray photoelectron spectroscopy (XPS)/Fourier-transform infrared spectroscopy (FTIR) analysis uncover several chemistry-related insights associated with Mg-based promotion. Importantly, the three-phase line of magnesium−water−CO_2 gas is key to promotion. Porous oxide layers, generation of H_2 nanobubbles, and chemisorption of CO_2 on Mg surfaces are other factors responsible for accelerated nucleation. Interestingly, Mg alloys exhibit faster nucleation promotion than pure Mg, which is significant in salt water medium. Overall, our work opens up pathways for faster synthesis of hydrates, which is critical to realizing applications.

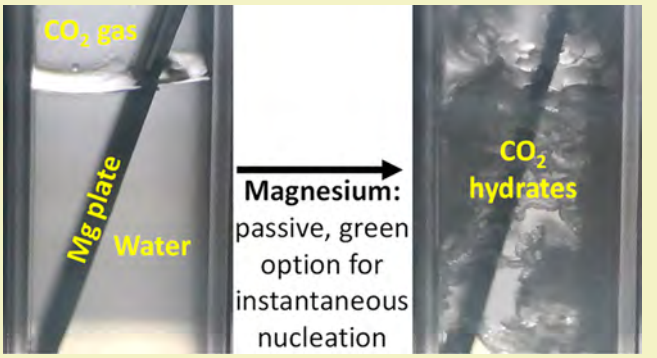

KEYWORDS: *CO_2 hydrates, nucleation, magnesium, induction time, magnesium alloy, magnesium oxide, nanobubbles*

INTRODUCTION

Gas hydrates are icelike crystalline solids consisting of cages of water molecules enclosing a "guest molecule" and form under high-pressure, low-temperature conditions. CO_2 hydrates offer a promising and novel route to large-scale decarbonization,[1] wherein CO_2 from industrial processes, or CO_2 extracted from the air, could be used to synthesize CO_2 hydrates and then sequestered (stored) in geologic formations under the ocean floor.[1] Gas hydrates have also been proposed as solutions in other diverse areas such as desalination, gas separation, gas storage, transportation, etc.[2−4] The potential of hydrates as solutions to multiple environmental and sustainability-related issues can only be realized by overcoming multiple thermodynamic and kinetic challenges to the synthesis of gas hydrates.[5] Slow nucleation of hydrates is one of the key challenges associated with hydrate formation. Nucleation refers to the formation of the first "stable" crystal of hydrate that can subsequently grow.[6−9] While nucleation is undoubtedly influenced by thermodynamic conditions, the induction (wait) time for hydrates to nucleate can range from hours to days in the absence of any external promotion techniques.[10] Additional key challenges associated with hydrate formation involve slow growth rates and low gas-to-hydrate conversion. We note that the present group recently published a related article on the kinetics of film growth of hydrates.[11]

There have been several advancements to address this well-known issue of highly stochastic, long induction times. Surfactants, ionic liquids, and proteins are well-known kinetic promoters that accelerate the rate of hydrate nucleation.[12−22] Traditionally, anionic surfactants such as sodium dodecyl sulfate (SDS) have been used to effectively promote nucleation.[23−28] However, in general, surfactants are not considered environmentally friendly, are expensive, and lead to process-related issues due to foaming. Alternatively, mechanical stirring can significantly decrease the nucleation time; however, it increases the complexity of the high-pressure reactor in terms of plugging and requires energy input.[26,29,30]

Received: May 6, 2021
Revised: July 27, 2021

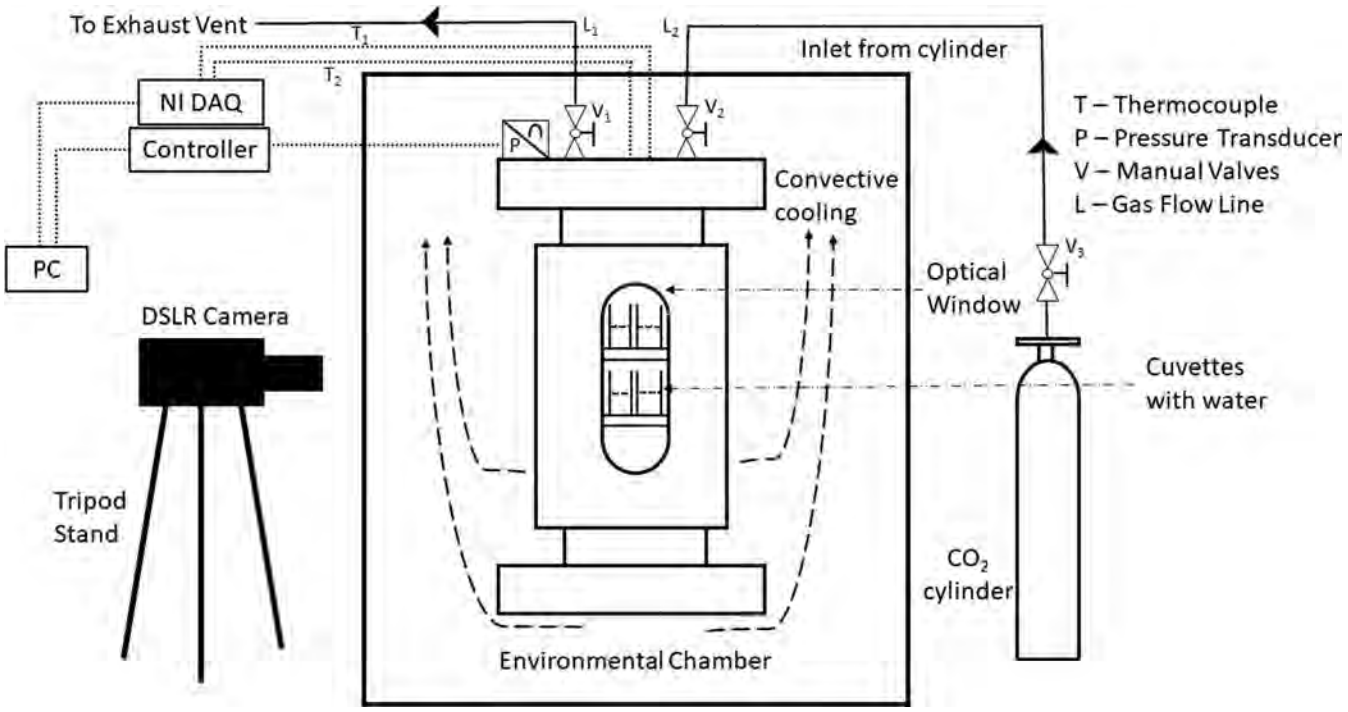

Figure 1. Schematic illustration of the experimental setup.

Thermodynamic promoters, which alter the hydrate equilibrium curve, can also influence the induction time for hydrate nucleation.[31−34] Thermodynamic promoters are often combined with kinetic promoters to enhance hydrate formation.[35−38] However, these promoters again involve the use of chemicals such as tetra-*n*-butylammonium bromide (TBAB) or tetrahydrofuran (THF), which are often required in large quantities and not considered environmentally friendly. Other methods, such as utilizing hydrate seeds, supersaturation, ice melts, amino acids, electronucleation, and acoustics have also been studied to facilitate the nucleation of hydrates.[39−45] Electronucleation has been studied by the authors of this study: even though it can enable fast nucleation, it introduces additional complexities in the reactor.[45]

There have been a limited number of studies on surface-promoted nucleation of hydrates (a passive technique for nucleation promotion). Metals and metal oxide suspensions have been experimentally shown to assist in nucleation promotion and have also been studied in conjunction with surfactants.[46−64] Passive promotion and the underlying mechanisms have also been studied via molecular dynamics simulations.[65−69] A recent discovery by the present group involved the use of aluminum surfaces to promote the nucleation of CO_2 hydrates.[70] Statistically significant measurements showed CO_2 hydrates nucleating in ∼3 h on aluminum surfaces (with no nucleation observed in the absence of aluminum). It was hypothesized that hydrogen bubbles generated at the aluminum−water interface were responsible for such promotion.

Presently, we report that magnesium (Mg) can induce nucleation of CO_2 hydrates within a few minutes; this represents a 500 times increase in nucleation rate, compared to our previous results on aluminum-based promotion.[70] Our best current results show nucleation occurring in less than 1 min, which is very close to the instantaneous, on-demand nucleation that is required for practical applications. Carefully conducted experiments and direct visualization of nucleation enable statistically meaningful measurements of nucleation, which are often lacking in literature. Both pure Mg and a common Mg alloy (AZ31) result in significant nucleation promotion with the use of pure or salt water. X-ray photoelectron spectroscopy (XPS) and Fourier-transform infrared spectroscopy (FTIR) measurements provide insights into the interfacial chemistry and reactions that result in such accelerated nucleation. Overall, this work has uncovered a novel and passive technique for ultrafast CO_2 hydrate nucleation.

EXPERIMENTAL SETUP

Figure 1 shows a schematic of the experimental setup. A custom-built, 450 mL pressure vessel (Parr Instruments) with sapphire windows (for visualization) was used. Experiments were conducted in 3 mL capacity polystyrene spectrophotometric cuvettes; four cuvettes could be accommodated and visualized per experiment. The pressure vessel was located in an environmental chamber (ESPEC). Hydrate nucleation was visually detected using a Nikon DSLR 850 camera fitted with a Tokina macro lens. The temperature was monitored with T-type, 1 mm diameter grounded thermocouples (Omega) connected to a DAQ (National Instruments). Mirror-polished (surface roughness: 137 nm) Mg alloy (AZ31) plates (from Goodfellow) and pure Mg rods (99.9% purity, from Sigma-Aldrich) were used. The Mg alloy plates had dimensions of 28 mm by 6.25 mm with a thickness of 1 mm, whereas the pure Mg rods were 28 mm long with a diameter of 1.5 mm. The Mg alloy had a bulk composition of 96% Mg, 3% Al, and 1% Zn with tolerances within 5%.

All surfaces were cleaned with deionized (DI) water and isopropyl alcohol followed by drying with nitrogen gas (99.99% purity). All experiments were conducted at 1 °C and 475 psi (3.28 MPa), which avoids any possibility of ice formation. After Mg was placed in cuvettes filled with water, the pressure vessel was first purged with CO_2 gas at 15 psi to remove air. The temperature in the pressure vessel was then stabilized to 1 °C, by allowing it to rest for 1 h; this eliminates any temperature gradients inside the pressure vessel. The temperature was measured using two thermocouples, one placed near the top of the vessel and the other near the center. After thermal

https://doi.org/10.1021/acssuschemeng.1c03041
ACS Sustainable Chem. Eng. XXXX, XXX, XXX−XXX

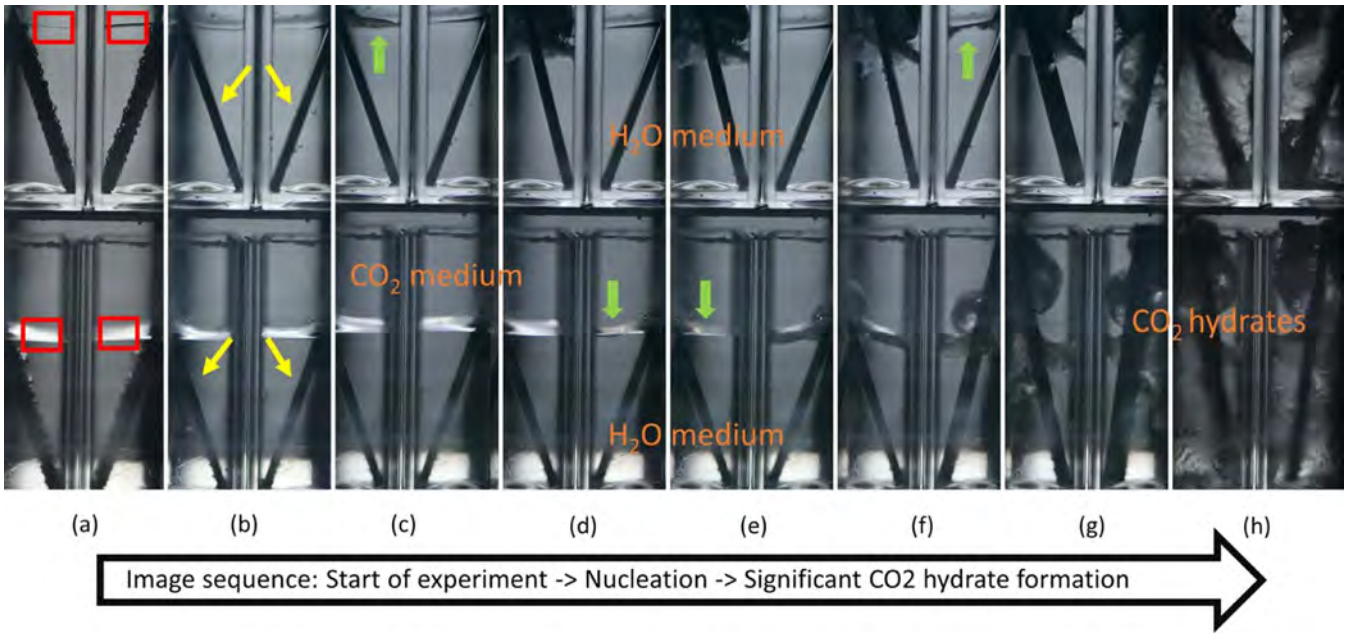

Figure 2. Time-lapse image sequence showing hydrate formation. Four cuvettes partially filled with water and containing an inclined Mg alloy plate each, are shown in each image from (a–h). Red squares show the CO_2 gas–water interface and yellow arrows show the Mg alloy plates. The specific state of each image is as follows: (a) temperature of 1 °C, just before pressurization. (b) Just after pressurization with CO_2 to 475 psi at 1 °C. (c–f) Green arrows show the nucleation location of CO_2 hydrates on the CO_2 gas–water interface of each cuvette. Each image is just after nucleation on the respective cuvette. Nucleation occurs at different times reflecting the stochastic nature of the behavior. (g) Hydrate growth after 15 min of pressurization. (h) Significant conversion of water to CO_2 hydrates after 45 min.

equilibration, both thermocouples measured 1 °C with an accuracy of ±0.2 °C. After the rest period, the vessel was pressurized by CO_2 (99.99% purity) to 475 psi. Induction time was estimated from the time that the temperature and pressure conditions entered the thermodynamic hydrate stability region, based on the equilibrium curve of CO_2 hydrate formation.[10] The data reported in this study is the average of eight repeats for a particular configuration. More details on the experimental procedure are available in the Supporting Information.

RESULTS AND DISCUSSION

Nucleation Experiments in Cuvettes. Figure 2 shows images of CO_2 hydrate formation in four cuvettes (in one experiment) containing inclined Mg alloy plates. The configuration of the plate is shown in Figure 3a and pure Mg rods also had a similar configuration. A sequence of time-lapse images is shown with significant hydrate formation observed in the last image (Figure 2h). Nucleation is seen to occur in each of the four cuvettes at various times (highlighted by the green arrow in Figure 2c–f). This direct visualization allows accurate detection of nucleation and measurement of the induction time. We note that getting high-quality, high-magnification images is very challenging in such high-pressure, confined access systems. Video 1 in the Supporting Information shows nucleation occurring inside the cuvettes.

Table 1 summarizes the induction time measurements from this work. No nucleation was detected even after 15 h in the control experiments (no Mg). In contrast, both pure Mg and Mg alloy exhibited significant nucleation promotion, with average nucleation times of ∼13 and ∼9 min, respectively, with minimum nucleation times of ∼7 to 8 min. Interestingly, nucleation was always observed to initiate at the three-phase contact line of water–CO_2 gas–Mg. Video 1 included in the Supporting Information clearly captures this phenomenon. There was no influence of the volume of water (in the cuvette) on the nucleation time as long as the three-phase contact line was in play. Furthermore, pure Mg resulted in higher nucleation times than Mg alloy; a hypothesis to explain this difference is outlined later. Data on all of the induction time measurements is included in the Supporting Information.

Similar experiments were also conducted with sodium chloride solutions (concentration of 35 g/L) to mimic CO_2 hydrate formation in seawater. This is an important consideration since applications such as oceanic sequestration of CO_2 and seawater desalination will involve hydrate formation with salt water. The average nucleation time showed a significant increase to ∼24 min and ∼2 h for Mg alloy and pure Mg, respectively, with minimum nucleation times of ∼11 to 19 min (Table 1). This increase is expected and can be attributed to the salt-induced shift in the equilibrium temperature of hydrate formation.[71,72] Dissociation of ionic salts creates hydration shells, which makes it harder for water molecules to orient suitably for hydrate formation. It is noted that the average induction time for Mg alloy is still very favorable (compared to state of the art); however, it is significantly higher for pure Mg. Possible mechanisms, which explain this difference, are outlined in a subsequent section.

Next, we have investigated the influence of the three-phase line and geometrical configurations of the Mg alloy plate on nucleation. Figure 3a–d shows the different configurations of Mg alloy plates. Table 2 shows the induction time comparison of all of these configurations. First, the average nucleation time increased from ∼9 min for the configuration in Figure 3a to ∼46 min for the configuration in Figure 3b. The configuration in Figure 3a has the three-phase contact line of water–CO_2 gas–Mg, whereas the configuration in Figure 3b does not, since the Mg plate is completely submerged. Very interestingly, nucleation for the configuration in Figure 3b was observed to originate not on the Mg plate, but rather near the three-phase

https://doi.org/10.1021/acssuschemeng.1c03041
ACS Sustainable Chem. Eng. XXXX, XXX, XXX–XXX

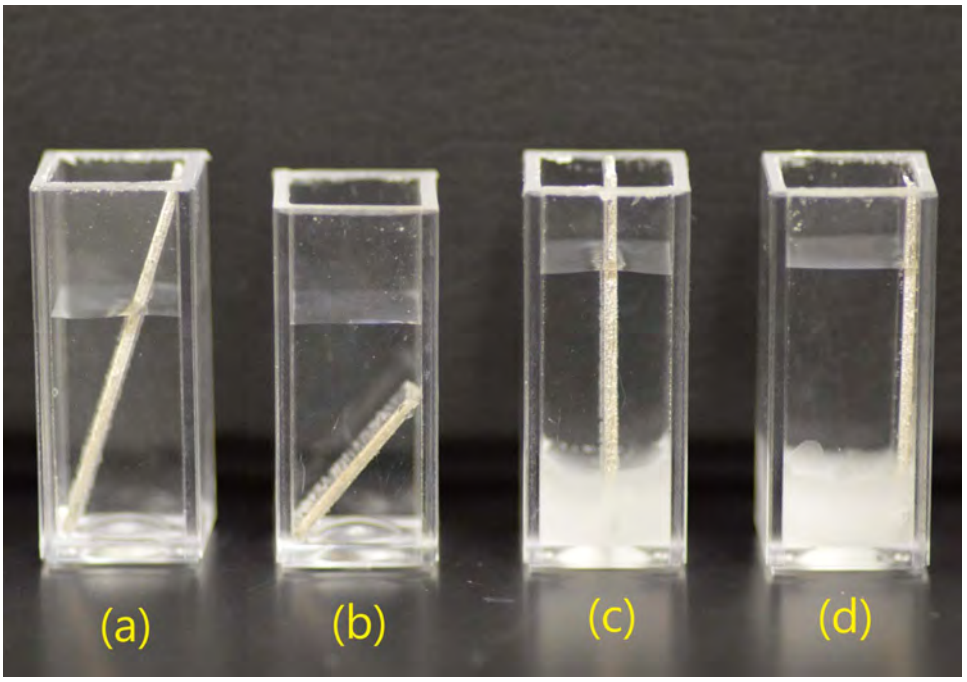

Figure 3. Various configurations of Mg alloy plates. (a) Inclined Mg alloy plate, (b) Mg alloy plate completely submerged, (c) upright and centered Mg alloy plate, and (d) Mg alloy plate upright and flush with side wall of the cuvette.

Table 1. Summary of Induction Time Data for Various Experiments with Mg alloy and pure Mg.

promoter	water	mean induction time (min)	standard deviation (min)	minimum induction time (min)	maximum induction time (min)
Mg alloy plate (AZ31)	pure	8.76	0.90	7.3	10.0
	salt water (35 g/L)	23.52	7.40	11.0	29.5
pure Mg rod	pure	13.26	4.21	7.9	20.8
	salt water (35 g/L)	120.78	93.77	19.4	239.6
none	pure	no nucleation (>15 h)			
	salt water (35 g/L)	no nucleation (>15 h)			

Table 2. Summary of Induction Times for Various Configurations of Mg Alloy Plates[a]

configuration	mean induction time (min)	standard deviation (min)	minimum induction time (min)	maximum induction time (min)
inclined (a)	8.76	0.90	7.3	10.0
immersed—no three-phase line (b)	46.4	4.21	37	50.1
upright and centered (c)	10.36	1.77	8.8	13.5
upright and flush with side (d)	2.92	1.96	1.12	6.47

[a]Configurations (a)−(d) are shown in Figure 3.

contact line of the cuvette surface (water−CO_2 gas−polystyrene). It is likely that magnesium oxide particles attached to the rising hydrogen gas bubbles (generated on the Mg surface) trigger nucleation on the gas−water interface. These gas bubbles can be seen in Video 2 (included as the Supporting Information) and are generated due to the reaction of Mg with water, as discussed in a later section. We note that a previous study analyzed the influence of Mg oxide powders (assisted by mechanical stirring) on the nucleation of natural gas hydrates.[56] Our findings clearly highlight the importance of the three-phase contact line on nucleation; this aspect of nucleation has also been captured in molecular dynamics (MD) simulations.[73] We note that nucleation of hydrates can sometimes occur inside bulk water for supersaturated systems.[74,75] However, in our setup, the bulk of water was largely undersaturated due to the absence of stirring and surfactants.

Next, we outline the configuration which resulted in the fastest nucleation in the cuvette-based experiments. Figure 3c,d shows upright Mg alloy plates protruding above the water level, with the plate in Figure 3c being centered, while the plate in Figure 3d being flush against the polystyrene wall of the cuvette. The plates were maintained upright by cementing them at the bottom with paraffin wax. Control experiments were conducted with just paraffin wax and water (no Mg), where no nucleation was observed in 15 h. The centered plate (Figure 3c) did not show a significant difference in the nucleation time from the inclined plate configuration (Figure 3a). However, the configuration in Figure 3d showed a noticeably faster average nucleation time of 2.9 min (Table 2). In some experiments, it resulted in nucleation time as low as

https://doi.org/10.1021/acssuschemeng.1c03041
ACS Sustainable Chem. Eng. XXXX, XXX, XXX−XXX

1.1 min, which is a noteworthy finding for nucleation under stagnant conditions. Overall, placing the Mg alloy plate flush with the cuvette walls (such that the three-phase contact line exists) yields the fastest nucleation for CO_2 hydrates. We note that we expect gaps on the order of 100 μm between the plate surface and the cuvette wall. This suggests that confinement-related effects can possibly accelerate nucleation and are discussed later in the paper. Such promotion effects resulting from two surfaces in close vicinity have been experimentally reported for hydrate formation in porous media and have also been captured in MD simulations.[67,76,77] Mechanistic pathways captured through MD simulations show the formation of nanobubbles and stabilization of hydrate clusters through hydrogen bonding on the adjacent surfaces.

Finally, we compare Mg-based nucleation promotion of CO_2 hydrates with surfactant-based promotion via experiments with sodium dodecyl sulfate (SDS), which is widely used for promoting hydrate nucleation and growth. Two thousand parts per million solutions of SDS in DI water were placed in polystyrene cuvettes (no Mg) and the previously outlined experimental procedure was followed to induce nucleation. We measured induction times of about 5 h. The concentration of SDS was not varied, and it will indeed influence the nucleation time to a certain extent. However, the large difference in the induction times with Mg and with SDS clearly highlight the relative benefits of Mg over surfactants in promoting nucleation, noting that different mechanisms are at play for Mg-promoted and surfactant-promoted nucleation.

Nucleation Experiments with Larger Volumes of Water. While the experiments clearly highlight the promise of Mg in promoting CO_2 hydrate nucleation, they were conducted with only 1.5 mL of water. Additional experiments were conducted with larger water volumes to highlight the scalability of Mg-based nucleation promotion. The pressure vessel was filled up with 350 mL of water. A Mg alloy AZ31 plate (of the same size as those used in the cuvette-based experiments) was stuck to the side of the pressure vessel while ensuring that there exists a three-phase contact line of CO_2−water−Mg. This setup essentially mimicked the configuration in Figure 3d, where we observed the fastest nucleation. It is noted that despite scaling up the water volume by a factor of 233, the plate size was kept the same. The rest of the experimental procedure was the same as before.

Interestingly, these bulk water experiments revealed that CO_2 hydrates nucleated in 0.7 ± 0.1 min (based on eight experiments). CO_2 hydrates nucleated during the pressurization stage at pressures ranging between 350 and 400 psi. Nucleation occurred in the thermodynamic hydrate stability region (as discussed earlier) even before pressurization to 475 psi was complete. To the best of our knowledge, this is the fastest nucleation of any gas hydrate ever reported; the results are even more remarkable considering the complete absence of traditional approaches to trigger nucleation (surfactants, promoters, mechanical stirring, etc.). Control experiments conducted in the absence of the Mg alloy plate yielded nucleation times of 53 ± 17.1 min (based on eight experiments). These results clearly show that Mg can trigger near-instantaneous, on-demand nucleation of CO_2 hydrates. These results also reveal that Mg-based nucleation promotion is scalable. This should be expected since heterogeneous nucleation is a surface-dependent phenomenon and does not depend upon the volume of the reactor. Nucleation and the subsequent growth of the hydrate film on the gas−water interface in these experiments are shown in Video 3. Data on all of the induction time measurements is included in the Supporting Information.

Faster nucleation in a large volume reactor (350 mL of water) as compared to smaller-scale (1.5 mL of water) experiments in polystyrene cuvettes is a very noteworthy aspect of the present experiments. The size of the Mg alloy plate is the same in both experiments; therefore, the difference in nucleation times can be attributed to the stainless steel walls of the reactor. In large volume water experiments, the hydrophilic stainless steel walls likely work in conjunction with the Mg alloy plate to assist nucleation. The nucleation promotion influence of stainless steel has been reported in literature.[78−80] More research is needed to understand the synergistic influence of two different surfaces in close contact. However, it should be clear that the influence of Mg is much stronger than that of stainless steel.

Estimating Nucleation Rates from Induction Time Measurements. While the previous sections detailed the induction time benefits of Mg-assisted nucleation promotion, this section quantifies the measured nucleation rate. Comparison of the nucleation rate with those in other experiments is more meaningful than a direct comparison of induction times. Presently, we use a formulation (based on classical nucleation theory) developed by Maeda,[81,82] to estimate nucleation rates from the measured induction times. The method of determining nucleation rates relies on estimating survival probabilities as determined by eq 1. $F(t)$ is the survival probability, defined as the probability that a particular sample does not nucleate after time t. k is the nucleation rate which is determined from the slope of $\ln F(t)$ vs t. Additional details on this method are outlined in Maeda.[81,82] Since our experiments showed the three-phase contact line to be a key factor for nucleation, our estimates are based per unit length of the three-phase contact line.

$$\ln F(t) = -0.693kt \tag{1}$$

For the experimental results of nucleation in cuvettes, measurements indicate a nucleation rate of 1.2 Hz m^{-1} for the fastest nucleating configuration (Figure 3d), where the Mg plate is placed close to the reactor walls (with a three-phase contact line). In the absence of a Mg plate in the cuvette, no nucleation occurred in 15 h, and the nucleation rate would theoretically be zero (if we assume no nucleation). In the large volume water case (with reactor walls of stainless steel), the measured nucleation rates were larger. The average nucleation rate in the presence of Mg was ∼9.3 Hz m^{-1}. Since nucleation occurred during pressurization of the vessel, the reported nucleation rate is an average for a pressure of ∼380 psi. In the large volume experiments without Mg, the nucleation rate was 0.003 Hz m^{-1}. The observed enhancement factor due to Mg is therefore >3000.

We also provide comparisons with our previous work[70] on aluminum-based promotion; the measured induction times of a few hours translate to nucleation rates of 0.02 Hz m^{-1} (adjusted to relevant experimental conditions). Mg-based promotion is therefore ∼500 times faster than Al-based promotion.[70] We can also compare the present results with the comprehensive assessment of nucleation rates of CO_2 hydrates obtained by Maeda.[83] Mg-promoted nucleation rates from our present experiments (large water volume) are ∼70 times larger than Maeda's measurements using a HP-ALTA apparatus; this again highlights the benefits of Mg.

https://doi.org/10.1021/acssuschemeng.1c03041
ACS Sustainable Chem. Eng. XXXX, XXX, XXX−XXX

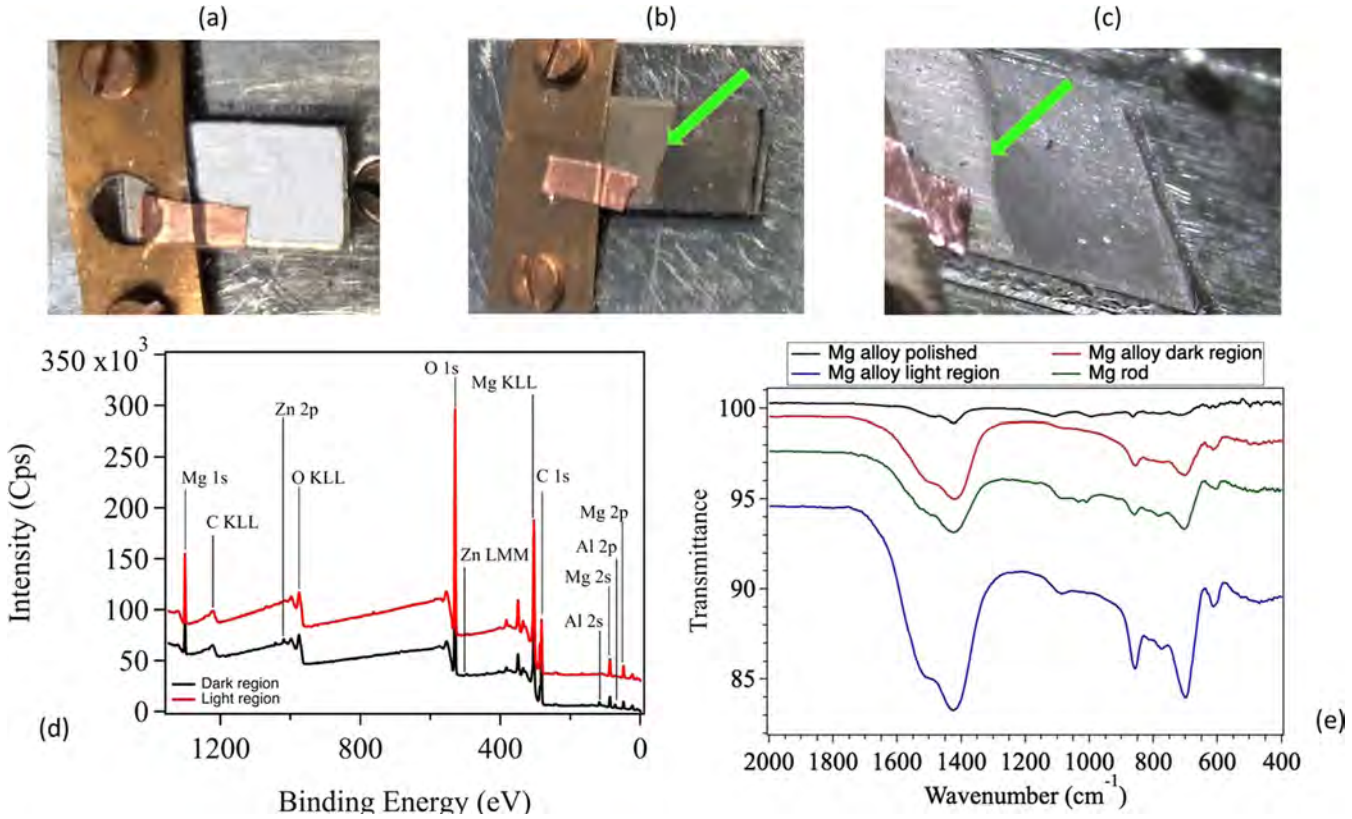

Figure 4. (a, b) Image of a Mg alloy plate held by a copper grounding prior to XPS characterization. Image (a) shows the Mg alloy plate before hydrate formation and image (b) shows the plate after hydrate formation. (c) Magnified view of the light to dark region on the Mg alloy plate where the water−gas interface was present. The tentative gas−water interface is marked with a green arrow. (d) Wide XPS spectra of Mg alloy plates post experiment, showing difference in compositions between light (unsubmerged) and dark (submerged) regions. The peaks are marked according to the binding energies of different elements. (e) Plot shows the FTIR spectra depicting strong absorption bands at 1420 cm^{-1} due to the presence of carbonates and bicarbonates on postexperiment Mg alloy plates and pure Mg rods.

Interestingly, our baseline nucleation rates (without the presence of Mg) are lower than those reported by Maeda.[83] We recognize that we have only eight sets of measurements per experimental configuration, which is not a very large sample size from a statistical standpoint. Nevertheless, the obtained results do highlight the benefits of Mg, as highlighted by a comparison of the nucleation rates.

Understanding the Mechanisms Underlying Nucleation. This section discusses various aspects of the experimental results and possible mechanisms and hypothesis underlying the Mg-based nucleation promotion. XPS and FTIR characterization of pure Mg and Mg alloy surfaces was conducted post experiments to obtain insights into the chemical composition on the surface. XPS spectra were recorded using a commercial X-ray photoelectron spectrometer (Kratos Axis Ultra DLD, Manchester, U.K.), utilizing a monochromated Al Ka X-ray source ($h\nu$ = 1486.5 eV), hybrid optics (employing a magnetic and electrostatic lens simultaneously), and a multichannel plate coupled to a hemispherical photoelectron kinetic analyzer. The base pressure in the analysis chamber was ~5×10^{-9} Torr. The spectrometer was calibrated according to ISO 15472:2001 with an accuracy better than ±0.05 eV. Spectra were collected with a pass energy of 20 at 0.1 eV per step, and four sweeps. Casa XPS analysis software was used for peak analysis and the stoichiometry of samples was determined using the procedure outlined in Mangolini et al..[84] All peaks were calibrated with respect to the metallic Mg signal at 49.6 eV. FTIR spectra were collected with a commercial FTIR (model Infinity Gold FTIR manufactured by Thermo Mattson). Spectra were obtained using a liquid nitrogen cooled Narrow Band MCT detector (700−4800 cm^{-1}) and collected 256 scans at 4 cm^{-1} resolution. An attenuated total reflection cell (ATR, model MIRacle single reflection manufactured by Pike Technologies), equipped with Ge crystal, was used to collect all spectra under ambient conditions.

Post experiments, the Mg alloy plates showed two distinctly colored regions, where the part immersed under water was much darker than the part exposed to CO_2 gas (Figure 4a−c). A wide XPS spectra (Figure 4d) on the two regions revealed the presence of minor alloying elements, Zinc (Zn) and aluminum (Al), on the surface of the dark region, which was absent on the light region. The presence of Zn and Al makes the dark (submerged) region resistant to corrosion−erosion. Corrosion is an exothermic process,[85] which will raise the temperature locally and delay nucleation if the heat dissipation from the site is slow. This finding also offers an explanation for the faster nucleation on Mg alloy plates, as compared to pure Mg rods (Table 1). Pure Mg (which did not have the corrosion−erosion protection accorded by Al and Zn) was seen (visually) to erode, thereby raising the local temperature and slowing down nucleation. This erosion was especially severe in salt water, with the resulting oxide layer seen to peel off eventually. Pure Mg resulted in average nucleation times of ~2 h compared to ~24 min of Mg alloy. Our findings suggest that corrosion/erosion resistant Mg alloys would be better candidates for nucleation promotion than pure Mg, especially

https://doi.org/10.1021/acssuschemeng.1c03041
ACS Sustainable Chem. Eng. XXXX, XXX, XXX−XXX

in offshore, marine environments. It is noted that such distinctly colored regions were absent on the pure magnesium rods, post experimentation.

High-resolution XPS spectra of the peaks could not be obtained accurately, hence, any knowledge of the oxidation states of the elements was not reliable. Strong distortion of the peaks and abnormal peak positions were observed due to differential charging of the surfaces. Such differential charging effects can be attributed to the porous oxide layers on the Mg surface, which creates a nonuniform electric field in the vicinity of the surface. However, FTIR spectra revealed interesting information on the functional groups present on the surface. FTIR spectra obtained on both pure Mg rods and Mg alloy plates (postreaction) showed CO_2 chemisorption on the surfaces. Strong absorption peaks at wavenumber 1420 cm^{-1} with an intense shoulder at higher wavenumbers indicate the presence of significant carbonate and bicarbonate groups on the surface as shown in Figure 4e. Such absorption peaks were absent on Mg surfaces before the experiment. It is noted that multiple studies[56,86−91] suggest that carbon adsorption on surfaces promotes nucleation of hydrates formed from hydrocarbons. Our results show that such surface chemisorption assists in nucleation promotion of CO_2 hydrates as well.

One highlight of the experimental results (Table 2) was the importance of the three-phase contact line of Mg−water−CO_2 in reducing the induction time. Contact line-based promotion can be attributed to a rich CO_2 aqueous phase present in the vicinity of the three-phase line and also to the generation of surface nanobubbles of hydrogen in the porous oxide layers of Mg.[92] These nanobubbles are generated due to the slow displacement reaction of water with Mg. Nanobubbles provide high-pressure points for heterogeneous nucleation on the oxide surface. The influence of bubbles on nucleation has been previously observed by our group, and bubble-promoted nucleation has been hypothesized in several other studies.[70,93−99] In particular, Li and Wang clearly concluded that the three-phase contact line helps in nucleation promotion of methane hydrates.[95]

The key result in Table 2 is the significant reduction in nucleation time if the Mg alloy plate is placed very close to the cuvette surface. These findings are complemented by the results of experiments conducted with 350 mL of water, in which nucleation consistently occurred in less than 1 min. While we do not study the phenomena resulting in such rapid nucleation, it is possible that capillary-related effects[100−102] in narrow spaces (gap between plate and cuvette surface) could be responsible. Another possibility is the influence of confinement on nucleation, noting that the role of confinement on hydrate formation has been previously studied.[67,77]

A natural extension of this work is to study Mg-promoted nucleation of other hydrate formers like methane. Mechanisms underlying nucleation promotion will be different for methane hydrates. As an illustration, methane would not corrode the surface of Mg significantly, as CO_2 does, methane solubility in water is lower than that of CO_2, and methane adsorption on Mg surfaces would be lower; however, bubble generation on Mg surfaces should still act as a promoting mechanism.

CONCLUSIONS

Presently, we describe the significant benefits of pure Mg and Mg alloy AZ31 for promoting the nucleation of CO_2 hydrates. Results from more than 80 experiments clearly demonstrate that Mg-based promotion can trigger hydrate nucleation in a few minutes, with the fastest nucleation obtained in less than a minute. The importance of this discovery is magnified by the complete absence of any other traditional nucleation-promoting technique (surfactants, chemicals, stirring, etc.). Importantly, this concept is promising at larger volumes. Our experiments affirm the importance of the three-phase line in nucleation promotion. Additionally, our experimental and surface characterization efforts suggest multiple interfacial phenomena that harmoniously work to achieve ultrafast nucleation. Overall, we believe that this simple and passive alternative for nucleation promotion opens up new avenues for faster hydrate formation, which is critical to realizing the benefits of hydrates in practical applications.

ASSOCIATED CONTENT

Supporting Information

The Supporting Information is available free of charge at https://pubs.acs.org/doi/10.1021/acssuschemeng.1c03041.

Details of the experimental procedure, a compilation of all of the data obtained in our experiments, and an illustrative plot utilized for the calculation of nucleation rates (PDF)

Shows the nucleation of CO_2 hydrates using Mg alloy plates in a cuvette (Video 1) (AVI)

Shows gas bubbles forming and rising on Mg plates (Video 2) (AVI)

Shows the nucleation of CO_2 hydrates using Mg alloy plates in large-scale experiments (Video 3) (AVI)

AUTHOR INFORMATION

Corresponding Author

Vaibhav Bahadur − *Walker Department of Mechanical Engineering, The University of Texas at Austin, Austin, Texas 78712, United States; Texas Materials Institute, The University of Texas at Austin, Austin, Texas 78712, United States;* orcid.org/0000-0001-7442-7769; Email: vb@austin.utexas.edu

Authors

Aritra Kar − *Walker Department of Mechanical Engineering, The University of Texas at Austin, Austin, Texas 78712, United States*

Palash Vadiraj Acharya − *Walker Department of Mechanical Engineering, The University of Texas at Austin, Austin, Texas 78712, United States*

Awan Bhati − *Walker Department of Mechanical Engineering, The University of Texas at Austin, Austin, Texas 78712, United States*

Ashish Mhadeshwar − *ExxonMobil Research and Engineering, Annandale, New Jersey 08801, United States*

Pradeep Venkataraman − *ExxonMobil Upstream Research Company, Spring, Texas 77389, United States*

Timothy A. Barckholtz − *ExxonMobil Research and Engineering, Annandale, New Jersey 08801, United States*

Hugo Celio − *Texas Materials Institute, The University of Texas at Austin, Austin, Texas 78712, United States*

Filippo Mangolini − *Walker Department of Mechanical Engineering, The University of Texas at Austin, Austin, Texas 78712, United States; Texas Materials Institute, The University of Texas at Austin, Austin, Texas 78712, United States;* orcid.org/0000-0003-3360-9122

https://doi.org/10.1021/acssuschemeng.1c03041
ACS Sustainable Chem. Eng. XXXX, XXX, XXX−XXX

Complete contact information is available at:
https://pubs.acs.org/10.1021/acssuschemeng.1c03041

Author Contributions

V.B. supervised the work and directed the project. A.K., V.B., A.M., P.V., and T.A.B. conceptualized the work. A.K. conducted the hydrate nucleation experiments and analyzed data. A.K. and V.B. devised the methods and wrote the original draft of the paper. A.K. and P.V.A. prepared the experimental setup for hydrate nucleation. H.C. conducted XPS and FTIR experiments. F.M. analyzed the XPS and FTIR data. A.B., A.M., P.V.A., P.V., T.A.B., and F.M. validated, reviewed, and edited the paper.

Notes

The authors declare the following competing financial interest(s): A US patent application related to the discovery reported in this work has been filed with USPTO by The University of Texas at Austin and ExxonMobil Research and Engineering.

■ ACKNOWLEDGMENTS

Research on CO_2 hydrates was supported by ExxonMobil through its membership in The University of Texas at Austin Energy Institute. This acknowledgment should not be considered an endorsement of the results by ExxonMobil. V.B. acknowledges NSF-CBET grant 1653412 for partial support of this work. The authors also acknowledge the support provided by Jamie and Israel from the machine shop in the Department of Mechanical Engineering.

■ REFERENCES

(1) Zheng, J.; Chong, Z. R.; Qureshi, M. F.; Linga, P. Carbon Dioxide Sequestration via Gas Hydrates: A Potential Pathway toward Decarbonization. *Energy and Fuels* **2020**, *34*, 10529−10546.
(2) Wang, X.; Zhang, F.; Lipinski, W. Research progress and challenges in hydrate-based carbon dioxide capture applications. *Appl. Energy* **2020**, *269*, 114928−114954.
(3) Leung, D. Y. C.; Caramanna, G.; Maroto-Valer, M. M. An Overview of Current Status of Carbon Dioxide Capture and Storage Technologies. *Renewable Sustainable Energy Rev.* **2014**, *39*, 426−443.
(4) Babu, P.; Nambiar, A.; He, T.; Karimi, I. A.; Lee, J. D.; Englezos, P.; Linga, P. A Review of Clathrate Hydrate Based Desalination to Strengthen Energy-Water Nexus. *ACS Sustainable Chem. Eng.* **2018**, *6*, 8093−8107.
(5) Hassanpouryouzband, A.; Joonaki, E.; Farahani, M. V.; Takeya, S.; Ruppel, C.; Yang, J.; English, N. J.; Schicks, J. M.; Edlmann, K.; Mehrabian, H.; Aman, Z. M.; Tohidi, B. Gas hydrates in sustainable chemistry. *Chem. Soc. Rev.* **2020**, *49*, 5225−5309.
(6) Jacobson, L. C.; Hujo, W.; Molinero, V. Amorphous Precursors in the Nucleation of Clathrate Hydrates. *J. Am. Chem. Soc.* **2010**, *132*, 11806−11811.
(7) Khurana, M.; Yin, Z.; Linga, P. A Review of Clathrate Hydrate Nucleation. *ACS Sustainable Chem. Eng.* **2017**, *5*, 11176−11203.
(8) Ke, W.; Svartaas, T. M.; Chen, D. A Review of Gas Hydrate Nucleation Theories and Growth Models. *J. Nat. Gas Sci. Eng.* **2019**, *61*, 169−196.
(9) Liang, R.; Xu, H.; Shen, Y.; Sun, S.; Xu, J.; Meng, S.; Ron Shen, Y.; Tian, C. Nucleation and Dissociation of Methane Clathrate Embryo at the Gas−Water Interface. *Proc. Natl. Acad. Sci. U.S.A.* **2019**, *116*, 23410−23415.
(10) Sloan, E. D.; Koh, C. A. *Clathrates Hydrates of the Natural Gases*; 2nd ed.; Marcel Dekker Inc.: New York, 2008; pp 65−108.
(11) Kar, A.; Bhati, A.; Acharya, P.; Mhahdeshwar, A.; Venkatraman, P.; Barckholtz, T.; Bahadur, V. Diffusion-based modeling of film growth of hydrates on gas-liquid interfaces. *Chem. Eng. Sci.* **2021**, *234*, 116456−116464.
(12) Naullage, P. M.; Bertolazzo, A. A.; Molinero, V. How Do Surfactants Control the Agglomeration of Clathrate Hydrates? *ACS Cent. Sci.* **2019**, *5*, 428−439.
(13) Lv, X.; Lu, D.; Liu, Y.; Zhou, S.; Zuo, J.; Jin, H.; Shi, B.; Li, E. Study on Methane Hydrate Formation in Gas-Water Systems with a New Compound Promoter. *RSC Adv.* **2019**, *9*, 33506−33518.
(14) Wang, F.; Liu, G. Q.; Meng, H. L.; Guo, G.; Luo, S. J.; Guo, R. B. Improved Methane Hydrate Formation and Dissociation with Nanosphere-Based Fixed Surfactants As Promoters. *ACS Sustainable Chem. Eng.* **2016**, *4*, 2107−2113.
(15) Kumar, A.; Bhattacharjee, G.; Kulkarni, B. D.; Kumar, R. Role of Surfactants in Promoting Gas Hydrate Formation. *Ind. Eng. Chem. Res.* **2015**, *54*, 12217−12232.
(16) Sa, J. H.; Sum, A. K. Promoting Gas Hydrate Formation with Ice-Nucleating Additives for Hydrate-Based Applications. *Appl. Energy* **2019**, *251*, No. 113352.
(17) Zhong, Y.; Rogers, R. E. Surfactant Effects on Gas Hydrate Formation. *Chem. Eng. Sci.* **2000**, *55*, 4175−4187.
(18) Heydari, A.; Peyvandi, K. Study of Biosurfactant Effects on Methane Recovery from Gas Hydrate by CO2 Replacement and Depressurization. *Fuel* **2020**, *272*, No. 117681.
(19) Mitarai, M.; Kishimoto, M.; Suh, D.; Ohmura, R. Surfactant Effects on the Crystal Growth of Clathrate Hydrate at the Interface of Water and Hydrophobic-Guest Liquid. *Cryst. Growth Des.* **2015**, *15*, 812−821.
(20) Dicharry, C.; Diaz, J.; Torré, J. P.; Ricaurte, M. Influence of the Carbon Chain Length of a Sulfate-Based Surfactant on the Formation of CO_2, CH_4 and CO_2−CH_4 Gas Hydrates. *Chem. Eng. Sci.* **2016**, *152*, 736−745.
(21) Okutani, K.; Kuwabara, Y.; Mori, Y. H. Surfactant Effects on Hydrate Formation in an Unstirred Gas/Liquid System: An Experimental Study Using Methane and Sodium Alkyl Sulfates. *Chem. Eng. Sci.* **2008**, *63*, 183−194.
(22) Tian, L.; Wu, G. Cyclodextrins as Promoter or Inhibitor for Methane Hydrate Formation? *Fuel* **2020**, *264*, No. 116828.
(23) Wang, F.; Jia, Z. Z.; Luo, S. J.; Fu, S. F.; Wang, L.; Shi, X. S.; Wang, C. S.; Guo, R. B. Effects of Different Anionic Surfactants on Methane Hydrate Formation. *Chem. Eng. Sci.* **2015**, *137*, 896−903.
(24) Kwon, Y. A.; Park, J. M.; Jeong, K. E.; Kim, C. U.; Kim, T. W.; Chae, H. J.; Jeong, S. Y.; Yim, J. H.; Park, Y. K.; Lee, J. dong. Synthesis of Anionic Multichain Type Surfactant and Its Effect on Methane Gas Hydrate Formation. *J. Ind. Eng. Chem.* **2011**, *17*, 120−124.
(25) Kumar, A.; Sakpal, T.; Linga, P.; Kumar, R. Influence of Contact Medium and Surfactants on Carbon Dioxide Clathrate Hydrate Kinetics. *Fuel* **2013**, *105*, 664−671.
(26) Molokitina, N. S.; Nesterov, A. N.; Podenko, L. S.; Reshetnikov, A. M. Carbon Dioxide Hydrate Formation with SDS: Further Insights into Mechanism of Gas Hydrate Growth in the Presence of Surfactant. *Fuel* **2019**, *235*, 1400−1411.
(27) Naeiji, P.; Varaminian, F. Kinetic Study of Carbon Dioxide Hydrate Formation by Thermal Analysis in the Presence of Two Surfactants: Sodium Dodecyl Sulfate (SDS) and Lauryl Alcohol Ethoxylate (LAE). *J. Mol. Liq.* **2018**, *254*, 120−129.
(28) Du, J.; Li, H.; Wang, L. Effects of Ionic Surfactants on Methane Hydrate Formation Kinetics in a Static System. *Adv. Powder Technol.* **2014**, *25*, 1227−1233.
(29) Li, A.; Jiang, L.; Tang, S. An Experimental Study on Carbon Dioxide Hydrate Formation Using a Gas-Inducing Agitated Reactor. *Energy* **2017**, *134*, 629−637.
(30) Douïeb, S.; Fradette, L.; Bertrand, F.; Haut, B. Impact of Fluid Flow Conditions on the Formation Rate of Carbon Dioxide Hydrates in a Semi-Batch Stirred Tank Reactor. *AIChE J.* **2015**, *61*, 4387−4401.
(31) Mech, D.; Sangwai, J. S. Phase Equilibrium of the Methane Hydrate System in the Presence of Mixed Promoters (THF + TBAB) and the Effect of Inhibitors (NaCl, Methanol, and Ethylene Glycol). *J. Chem. Eng. Data* **2016**, *61*, 3607−3617.
(32) Herslund, P. J.; Thomsen, K.; Abildskov, J.; von Solms, N.; Galfré, A.; Brântuas, P.; Kwaterski, M.; Herri, J. M. Thermodynamic Promotion of Carbon Dioxide-Clathrate Hydrate Formation by

Tetrahydrofuran, Cyclopentane and Their Mixtures. *Int. J. Greenhouse Gas Control* **2013**, *17*, 397−410.
(33) Torré, J. P.; Haillot, D.; Rigal, S.; De Souza Lima, R.; Dicharry, C.; Bedecarrats, J. P. 1,3 Dioxolane versus Tetrahydrofuran as Promoters for CO_2-Hydrate Formation: Thermodynamics Properties, and Kinetics in Presence of Sodium Dodecyl Sulfate. *Chem. Eng. Sci.* **2015**, *126*, 688−697.
(34) Tariq, M.; Rooney, D.; Othman, E.; Aparicio, S.; Atilhan, M.; Khraisheh, M. Gas Hydrate Inhibition: A Review of the Role of Ionic Liquids. *Ind. Eng. Chem. Res.* **2014**, *53*, 17855−17868.
(35) Veluswamy, H. P.; Kumar, S.; Kumar, R.; Rangsunvigit, P.; Linga, P. Enhanced Clathrate Hydrate Formation Kinetics at near Ambient Temperatures and Moderate Pressures: Application to Natural Gas Storage. *Fuel* **2016**, *182*, 907−919.
(36) Mech, D.; Gupta, P.; Sangwai, J. S. Kinetics of Methane Hydrate Formation in an Aqueous Solution of Thermodynamic Promoters (THF and TBAB) with and without Kinetic Promoter (SDS). *J. Nat. Gas Sci. Eng.* **2016**, *35*, 1519−1534.
(37) Kumar, A.; Bhattacharjee, G.; Barmecha, V.; Diwan, S.; Kushwaha, O. S. Influence of Kinetic and Thermodynamic Promoters on Post-Combustion Carbon Dioxide Capture through Gas Hydrate Crystallization. *J. Environ. Chem. Eng.* **2016**, *4*, 1955−1961.
(38) Nesterov, A. N.; Reshetnikov, A. M. New Combination of Thermodynamic and Kinetic Promoters to Enhance Carbon Dioxide Hydrate Formation under Static Conditions. *Chem. Eng. J.* **2019**, *378*, No. 122165.
(39) Khandelwal, H.; Qureshi, M.; Zheng, J.; Venkatraman, P.; Barckholtz, T.; Mhadeshwar, A.; Linga, P. Effect of L-Tryptophan in promoting the kinetics of carbon dioxide hydrate formation. *Energy Fuels* **2021**, *35*, 649−658.
(40) Park, T.; Kwon, T. H. Effect of Electric Field on Gas Hydrate Nucleation Kinetics: Evidence for the Enhanced Kinetics of Hydrate Nucleation by Negatively Charged Clay Surfaces. *Environ. Sci. Technol.* **2018**, *52*, 3267−3274.
(41) Natarajan, V.; Kalogerakis, N.; Engineering, P. Induction Phenomena in Gas Hydrate. *Chem. Eng. Sci.* **1994**, *49*, 2075−2087.
(42) Jeong, K.; Metaxas, P. J.; Chan, J.; Kuteyi, T. O.; Aman, Z. M.; Stanwix, P. L.; Johns, M. L.; May, E. F. Hydrate Nucleation and Growth on Water Droplets Acoustically-Levitated in High-Pressure Natural Gas. *Phys. Chem. Chem. Phys.* **2019**, *21*, 21685−21688.
(43) Baek, S.; Ahn, Y. H.; Zhang, J.; Min, J.; Lee, H.; Lee, J. W. Enhanced Methane Hydrate Formation with Cyclopentane Hydrate Seeds. *Appl. Energy* **2017**, *202*, 32−41.
(44) Chen, B.; Dong, H.; Sun, H.; Wang, P.; Yang, L. Effect of a weak electric field on THF hydrate formation: Induction time and morphology. *J. Pet. Sci. Eng.* **2020**, *194*, No. 107486.
(45) Carpenter, K.; Bahadur, V. Electronucleation for Rapid and Controlled Formation of Hydrates. *J. Phys. Chem. Lett.* **2016**, *7*, 2465−2469.
(46) Kakati, H.; Mandal, A.; Laik, S. Promoting Effect of Al2O3 / ZnO-Based Nanofluids Stabilized by SDS Surfactant on CH4 + C2H6 + C3H8 Hydrate Formation. *J. Ind. Eng. Chem.* **2016**, *35*, 357−368.
(47) Nashed, O.; Partoon, B.; Lal, B.; Sabil, K. M.; Shariff, A. M. Investigation of Functionalized Carbon Nanotubes' Performance on Carbon Dioxide Hydrate Formation. *Energy* **2019**, *174*, 602−606.
(48) Li, J.; Liang, D.; Guo, K.; Wang, R. The Influence of Additives and Metal Rods on the Nucleation and Growth of Gas Hydrates. *J. Colloid Interface Sci.* **2005**, *283*, 223−230.
(49) Yan, S.; Dai, W.; Wang, S.; Rao, Y.; Zhou, S. Graphene Oxide: An Effective Promoter for CO_2 Hydrate Formation. *Energies* **2018**, *11*, No. 1756.
(50) Mohammadi, A.; Manteghian, M.; Haghtalab, A.; Mohammadi, A. H.; Rahmati-Abkenar, M. Kinetic Study of Carbon Dioxide Hydrate Formation in Presence of Silver Nanoparticles and SDS. *Chem. Eng. J.* **2014**, *237*, 387−395.
(51) Nashed, O.; Partoon, B.; Lal, B.; Sabil, K. M.; Shariff, A. M. Review the Impact of Nanoparticles on the Thermodynamics and Kinetics of Gas Hydrate Formation. *J. Nat. Gas Sci. Eng.* **2018**, *55*, 452−465.
(52) Rahmati-Abkenar, M.; Manteghian, M.; Pahlavanzadeh, H. Experimental and Theoretical Investigation of Methane Hydrate Induction Time in the Presence of Triangular Silver Nanoparticles. *Chem. Eng. Res. Des.* **2017**, *120*, 325−332.
(53) Arjang, S.; Manteghian, M.; Mohammadi, A. Effect of Synthesized Silver Nanoparticles in Promoting Methane Hydrate Formation at 4.7MPa and 5.7MPa. *Chem. Eng. Res. Des.* **2013**, *91*, 1050−1054.
(54) Aliabadi, M.; Rasoolzadeh, A.; Esmaeilzadeh, F.; Alamdari, A. M. Experimental Study of Using CuO Nanoparticles as a Methane Hydrate Promoter. *J. Nat. Gas Sci. Eng.* **2015**, *27*, 1518−1522.
(55) Li, J.; Liang, D.; Guo, K.; Wang, R.; Fan, S. Formation and Dissociation of HFC134a Gas Hydrate in Nano-Copper Suspension. *Energy Convers. Manage.* **2006**, *47*, 201−202.
(56) Nesterov, A. N.; Reshetnikov, A. M.; Manakov, A. Y.; Rodionova, T. V.; Paukshtis, E. A.; Asanov, I. P.; Bardakhanov, S. P.; Bulavchenko, A. I. Promotion and Inhibition of Gas Hydrate Formation by Oxide Powders. *J. Mol. Liq.* **2015**, *204*, 118−125.
(57) Zhou, S.; Jiang, K.; Zhao, Y.; Chi, Y.; Wang, S.; Zhang, G. Experimental Investigation of CO2 Hydrate Formation in the Water Containing Graphite Nanoparticles and Tetra-n-Butyl Ammonium Bromide. *J. Chem. Eng. Data* **2018**, *63*, 389−394.
(58) Zhou, S. D.; Yu, Y. S.; Zhao, M. M.; Wang, S. L.; Zhang, G. Z. Effect of Graphite Nanoparticles on Promoting CO_2 Hydrate Formation. *Energy and Fuels* **2014**, *28*, 4694−4698.
(59) Javidani, A. M.; Abedi-Farizhendi, S.; Mohammadi, A.; Hassan, H.; Mohammadi, A. H.; Manteghian, M. The Effects of Graphene Oxide Nanosheets and Al_2O_3 Nanoparticles on the Kinetics of Methane + THF Hydrate Formation at Moderate Conditions. *J. Mol. Liq.* **2020**, *316*, No. 113872.
(60) Liu, G. Q.; Wang, F.; Luo, S. J.; Xu, D. Y.; Guo, R. B. Enhanced Methane Hydrate Formation with SDS-Coated Fe_3O_4 Nanoparticles as Promoters. *J. Mol. Liq.* **2017**, *230*, 315−321.
(61) Yu, Y.; Xu, C.; Li, X. Evaluation of CO_2 Hydrate Formation from Mixture of Graphite Nanoparticle and Sodium Dodecyl Benzene Sulfonate. *J. Ind. Eng. Chem.* **2018**, *59*, 64−69.
(62) Choi, J. W.; Chung, J. T.; Kang, Y. T. CO_2 Hydrate Formation at Atmospheric Pressure Using High Efficiency Absorbent and Surfactants. *Energy* **2014**, *78*, 869−876.
(63) Wang, F.; Song, Y. M.; Liu, G. Q.; Guo, G.; Luo, S. J.; Guo, R. B. Rapid Methane Hydrate Formation Promoted by Ag&SDS-Coated Nanospheres for Energy Storage. *Appl. Energy* **2018**, *213*, 227−234.
(64) Abdi-Khanghah, M.; Adelizadeh, M.; Naserzadeh, Z.; Barati, H. Methane Hydrate Formation in the Presence of ZnO Nanoparticle and SDS: Application to Transportation and Storage. *J. Nat. Gas Sci. Eng.* **2018**, *54*, 120−130.
(65) Bai, D.; Chen, G.; Zhang, X.; Sum, A. K.; Wang, W. How Properties of Solid Surfaces Modulate the Nucleation of Gas Hydrate. *Sci. Rep.* **2015**, *5*, No. 12747.
(66) DeFever, R. S.; Sarupria, S. Surface Chemistry Effects on Heterogeneous Clathrate Hydrate Nucleation: A Molecular Dynamics Study. *J. Chem. Thermodyn.* **2018**, *117*, 205−213.
(67) He, Z.; Linga, P.; Jiang, J. CH_4 Hydrate Formation between Silica and Graphite Surfaces: Insights from Microsecond Molecular Dynamics Simulations. *Langmuir* **2017**, *33*, 11956−11967.
(68) Ma, R.; Zhong, H.; Li, L.; Zhong, J.; Yan, Y.; Zhang, J.; Liu, J. Molecular Insights into the Effect of a Solid Surface on the Stability of a Hydrate Nucleus. *J. Phys. Chem. C* **2020**, *124*, 2664−2671.
(69) DeFever, R. S.; Sarupria, S. Surface Chemistry Effects on Heterogeneous Clathrate Hydrate Nucleation: A Molecular Dynamics Study. *J. Chem. Thermodyn.* **2018**, *117*, 205−213.
(70) Acharya, P. V.; Kar, A.; Shahriari, A.; Bhati, A.; Mhadeshwar, A.; Bahadur, V. Aluminum-Based Promotion of Nucleation of Carbon Dioxide Hydrates. *J. Phys. Chem. Lett.* **2020**, *11*, 1477−1482.
(71) Mohammadi, A. H.; Tohidi, B. Prediction of Hydrate Phase Equilibria in Aqueous Solutions of Salt and Organic Inhibitor Using a Combined Equation of State and Activity Coefficient-Based Model. *Can. J. Chem. Eng.* **2005**, *83*, 865−871.

https://doi.org/10.1021/acssuschemeng.1c03041
ACS Sustainable Chem. Eng. XXXX, XXX, XXX−XXX

(72) Mohammadi, A. H.; Richon, D. Thermodynamic Modeling of Salt Precipitation and Gas Hydrate Inhibition Effect of Salt Aqueous Solution. *Ind. Eng. Chem. Res.* **2007**, *46*, 5074−5079.
(73) Bai, D.; Chen, G.; Zhang, X.; Wang, W. Nucleation of the CO_2 Hydrate from Three-Phase Contact Lines. *Langmuir* **2012**, *28*, 7730−7736.
(74) Natarajan, V.; Bishnoi, P. R.; Kalogerakis, N. Induction phenomena in gas hydrate nucleation. *Chem. Eng. Sci.* **1994**, *49*, 2075−2087.
(75) Fandiño, O.; Ruffine, L. Methane hydrate nucleation and growth from the bulk phase: Further insights into their mechanisms. *Fuel* **2014**, *117*, 442−449.
(76) Casco, M. E.; Silvestre-Albero, J.; Ramírez-Cuesta, A. J.; Rey, F.; Jordá, J. L.; Bansode, A.; Urakawa, A.; Peral, I.; Martínez-Escandell, M.; Kaneko, K.; Rodríguez-Reinoso, F. Methane Hydrate Formation in Confined Nanospace Can Surpass Nature. *Nat. Commun.* **2015**, *6*, No. 6432.
(77) Yu, K. B.; Yazaydin, A. O. Does Confinement Enable Methane Hydrate Growth at Low Pressures? Insights from Molecular Dynamics Simulations. *J. Phys. Chem. C* **2020**, *124*, 11015−11022.
(78) Stoporev, A. S.; Svarovskaya, L. I.; Strelets, L. A.; Altunina, L. K.; Manakov, A. Y. Effect of reactor wall material on the nucleation of methane hydrate in water-in-oil emulsions. *Mendeleev Commun.* **2018**, *28*, 343−344.
(79) Maeda, N. Nucleation curves of methane-propane mixed gas hydrates in the presence of a stainless steel wall. *Fluid Phase Equilib.* **2016**, *413*, 142−147.
(80) Abay, H. K.; Svartaas, T. H. Multicomponent gas hydrate nucleation: The effect of the cooling rate and composition. *Energy Fuels* **2011**, *25*, 42−51.
(81) Maeda, N. *Nucleation of gas hydrates*; Springer Nature: Switzeland AG, 2020.
(82) Maeda, N.; Shen, X. Scaling laws for nucleation rates of gas hydrates. *Fuel* **2019**, *253*, 1597−1604.
(83) Maeda, N. Nucleation curve of carbon dioxide hydrate from a linear cooling ramp method. *J. Phys. Chem. A* **2019**, *123*, 7911−7919.
(84) Mangolini, F.; Rossi, A.; Spencer, N. D. Chemical Reactivity of Triphenyl Phosphorothionate (TPPT) with Iron: An ATR/FT-IR and XPS Investigation. *J. Phys. Chem. C* **2011**, *115*, 1339−1354.
(85) Okonkwo, P. C.; Adel, M. A. M. Erosion-corrosion in oil and gas industry: a review. *Int. J. Metall. Mater. Sci. Eng.* **2014**, *4*, 7−28.
(86) Zhang, G.; Sun, M.; Liu, B.; Wang, F. Adsorption-Induced Two-Way Nanoconvection Enhances Nucleation and Growth Kinetics of Methane Hydrates in Confined Porespace. *Chem. Eng. J.* **2020**, *396*, No. 125256.
(87) Walsh, M. R.; Koh, C. A.; Sloan, E. D.; Sum, A. K.; Wu, D. T. Microsecond Simulations of Spontaneous Methane Hydrate Nucleation and Growth. *Science* **2009**, *326*, 1095−1098.
(88) He, Z.; Linga, P.; Jiang, J. What Are the Key Factors Governing the Nucleation of CO_2 Hydrate? *Phys. Chem. Chem. Phys.* **2017**, *19*, 15657−15661.
(89) Kyung, D.; Lim, H. K.; Kim, H.; Lee, W. CO_2 Hydrate Nucleation Kinetics Enhanced by an Organo-Mineral Complex Formed at the Montmorillonite-Water Interface. *Environ. Sci. Technol.* **2015**, *49*, 1197−1205.
(90) Casco, M. E.; Cuadrado-Collados, C.; Martinez-Escandell, M.; Rodriguez-Reinoso, F.; Silvestre-Albero, J. Influence of the oxygen-containing surface functional groups in the methane hydrate nucleation and growth in nanoporous carbon. *Carbon* **2017**, *123*, 299−301.
(91) Kashchiev, D.; Firoozabadi, A. Nucleation of gas hydrates. *J. Cryst. Growth* **2002**, *243*, 476−489.
(92) Alheshibri, M.; Qian, J.; Jehannin, M.; Craig, V. S. J. A History of Nanobubbles. *Langmuir* **2016**, *32*, 11086−11100.
(93) Kvamme, B.; Aromada, S. A.; Saeidi, N.; Hustache-Marmou, T.; Gjerstad, P. Hydrate Nucleation, Growth, and Induction. *ACS Omega* **2020**, *5*, 2603−2619.
(94) Kuang, Y.; Feng, Y.; Yang, L.; Song, Y.; Zhao, J. Effects of Micro-Bubbles on the Nucleation and Morphology of Gas Hydrate Crystals. *Phys. Chem. Chem. Phys.* **2019**, *21*, 23401−23407.
(95) Li, H.; Wang, L. Hydrophobized Particles Can Accelerate Nucleation of Clathrate Hydrates. *Fuel* **2015**, *140*, 440−445.
(96) Guo, Y.; Xiao, W.; Pu, W.; Hu, J.; Zhao, J.; Zhang, L. CH_4 Nanobubbles on the Hydrophobic Solid-Water Interface Serving as the Nucleation Sites of Methane Hydrate. *Langmuir* **2018**, *34*, 10181−10186.
(97) Zhang, Y.; Zhao, L.; Deng, S.; Zhao, R.; Nie, X.; Liu, Y. Effect of Nanobubble Evolution on Hydrate Process: A Review. *J. Therm. Sci.* **2019**, *28*, 948−961.
(98) Maeda, N. Interfacial Nanobubbles and the Memory Effect of Natural Gas Hydrates. *J. Phys. Chem. C* **2018**, *122*, 11399−11406.
(99) Bagherzadeh, S. A.; Alavi, S.; Ripmeester, J.; Englezos, P. Formation of methane nano-bubbles during hydrate decomposition and their effect on hydrate growth. *J. Chem. Phys.* **2015**, *142*, 214701−214709.
(100) Em, Y.; Stoporev, A.; Semenov, A.; Glotov, A.; Smirnova, E.; Villevald, G.; Vinokurov, V.; Manakov, A.; Lvov, Y. Methane hydrate formation in halloysite clay nanotubes. *ACS Sustainable Chem. Eng.* **2020**, *8*, 7860−7868.
(101) Daigle, H.; Dugan, B. Capillary controls on methane hydrate distribution and fracturing in advective systems. *Geochem., Geophys., Geosyst.* **2011**, *12*, No. Q01003.
(102) Zhang, Z.; Kusalik, P. G.; Guo, G. Bridging solution properties to gas hydrate nucleation through guest dynamics. *Phys. Chem. Chem. Phys.* **2018**, *20*, 24535−24538.

https://doi.org/10.1021/acssuschemeng.1c03041
ACS Sustainable Chem. Eng. XXXX, XXX, XXX−XXX